GEOLOGY | THE GEOLOGICAL SOCIETY OF AMERICA®

https://doi.org/10.1130/G46317.1

Manuscript received 29 March 2019
Revised manuscript received 15 September 2019
Manuscript accepted 17 September 2019

Published online 15 October 2019

Nanoscale evidence for temperature-induced transient rheology and postseismic fault healing

A.K. Ault[1]*, J.L. Jensen[1,2], R.G. McDermott[1], F.-A. Shen[3] and B.R. Van Devener[4]
[1]Department of Geosciences Utah State University, Logan, Utah 84322, USA
[2]ExxonMobil Upstream Business Development, Spring, Texas 77389, USA
[3]Microscopy Core Facility, Utah State University, Logan, Utah 84322, USA
[4]Nano-scale Imaging and Surface Analysis Laboratory, University of Utah, Salt Lake City, Utah 84112, USA

ABSTRACT

Friction-generated heat and the subsequent thermal evolution control fault material properties and thus strength during the earthquake cycle. We document evidence for transient, nanoscale fault rheology on a high-gloss, light-reflective hematite fault mirror (FM). The FM cuts specularite with minor quartz from the Pleistocene El Laco Fe-ore deposit, northern Chile. Scanning and transmission electron microscopy data reveal that the FM volume comprises a <50-μm-thick zone of polygonal hematite nanocrystals with spherical silica inclusions, rhombohedral twins, no shape or crystallographic preferred orientation, decreasing grain size away from the FM surface, and FM surface magnetite nanoparticles and Fe^{2+} suboxides. Sub–5-nm-thick silica films encase hematite grains and connect to amorphous interstitial silica. Observations imply that coseismic shear heating (temperature >1000 °C) generated transiently amorphous, intermixed but immiscible, and rheologically weak Fe-oxide and silica. Hematite regrowth in a fault-perpendicular thermal gradient, sintering, twinning, and a topographic network of nanometer-scale ridges from crystals interlocking across the FM surface collectively restrengthened fault material. Results reveal how temperature-induced weakening preconditions fault healing. Nanoscale transformations may promote subsequent strain delocalization and development of off-fault damage.

INTRODUCTION

Friction-generated heat activates various dynamic weakening mechanisms that lead to low coseismic fault strength (e.g., Rice, 2006; Di Toro et al., 2011; Goldsby and Tullis, 2011; Yao et al., 2016). Postseismic strength recovery of faults is observed in the field and laboratory and has been attributed to pressure solution (Yasuhara et al., 2005; Niemeijer et al., 2008), melt solidification (Mitchell et al., 2016; Proctor and Lockner, 2016), or fracture-sealing (Blanpied et al., 1992; Sibson, 1992). The extent to which various thermally activated dynamic weakening mechanisms seed fault healing, and the way in which nanoscale chemical and rheological changes govern these processes, and ultimately the seismic cycle, are unclear.

Exhumed faults provide a record of thermal, chemical, and rheological changes to fault materials by earthquake processes (Niemeijer et al., 2012; Rowe and Griffith, 2015). Fault mirrors (FM), common in fault damage zones, track these phenomena at micro- to nanoscales (e.g., Siman-Tov et al., 2013; Ault et al., 2015; Kuo et al., 2016; Pozzi et al., 2018). FMs are thin (<1 mm) high-gloss, light-reflective slip surfaces comprising layered nanoparticles, and they have been observed in carbonate, quartzite, granite, chert, and hematite (e.g., Power and Tullis, 1989; Fondriest et al., 2013; Kirkpatrick et al., 2013; Siman-Tov et al., 2013; Evans et al., 2014). Field studies and low- to high-speed deformation experiments on rock and gouge indicate FMs form by different processes and at variable slip rates (Verberne et al., 2013; Siman-Tov et al., 2015; McDermott et al., 2017; Pozzi et al., 2018).

Fault zones are mineralogically heterogeneous, and hematite is ubiquitous in these systems because iron is one of the most abundant elements in Earth's crust. Documenting the interplay among stress, strain, temperature, and hematite material properties informs fault system behavior. Here, we applied a suite of microscopy and spectroscopy tools to characterize nanotextures and nanogeochemistry, and thus infer thermal and rheological changes, to a hematite FM cutting Fe-ore. Observations are consistent with transient temperature rise and subsequent thermal decay during an earthquake. This thermal evolution controls weakening and, importantly, restrengthening of the FM during the seismic cycle.

SAMPLE AND METHODS

The Pliocene–Pleistocene El Laco Fe-ore deposit (67.48°W, 23.83°S) occurs on the flanks of an andesitic volcanic complex in northern Chile, and hosts magnetite, hematite, and apatite mineralization (Park, 1961; Naranjo et al., 2010; Tornos et al., 2017). The deposit is dissected by north-south– and northwest-southeast–oriented fault networks (Tornos et al., 2017). Our El Laco sample (A16–7) is a planar, metallic FM that cuts Fe-ore with a set of sub–millimeter-spaced slickenlines visible only at the FM margins (Fig. 1A; Fig. DR1 in the GSA Data Repository[1]).

We examined the texture and particle morphology of four cross-sectional and four surface (plan-view) millimeter- to centimeter-scale aliquots with scanning electron microscopy (SEM). SEM and Image J software (https://imagej.net/) were used to characterize the hematite grain-size distribution at and away from the FM. One cross-sectional and one plan-view

*E-mail: alexis.ault@usu.edu

[1]GSA Data Repository item 2020003, method details for sample preparation, scanning electron microscopy (SEM), electron-backscattered diffraction (EBSD) analysis, grain-size measurement, scanning/transmission electron microscopy (S/TEM), energy dispersive X-ray spectroscopy (EDS), and integrated EDS–electron energy loss spectroscopy (DualEELS), as well as SEM, EBSD, S/TEM, EDS, and DualEELS data/image catalogues, is available online at http://www.geosociety.org/datarepository/2020/, or on request from editing@geosociety.org.

CITATION: Ault, A.K., et al., 2020, Nanoscale evidence for temperature-induced transient rheology and postseismic fault healing: Geology, v. 48, p. 1203–1207, https://doi.org/10.1130/G46317.1

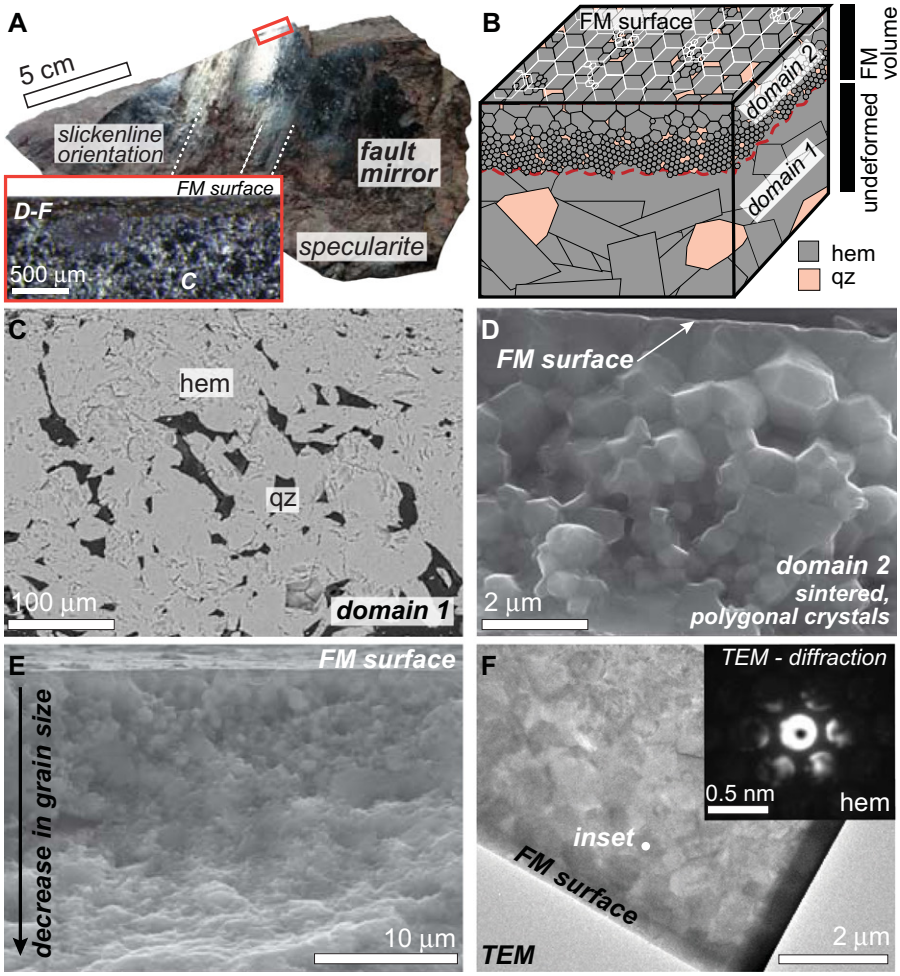

Figure 1. (A) Photograph of hematite fault mirror (FM) A16–7. Red box denotes location of inset, a cross-sectional aliquot photograph, showing scanning electron microscope (SEM) and transmission electron microscopy (TEM) image locations for C–F. (B) Schematic block diagram illustrating relationship and textures of two domains: domain 1—undeformed specularite; domain 2—FM volume and surface; hem—hematite; qz—quartz (domain 1; amorphous silica in domain 2). (C) SEM image away from FM with undeformed intergranular specular hematite and quartz. (D,E) Secondary election (SE) SEM cross-sectional images of FM showing sintered polygonal grains, flattened at FM interface (D) and FM-perpendicular decrease in polygonal grain size (E). (F) Upper domain 2 TEM image; inset is polygonal hematite single-crystal diffraction pattern.

aliquot were subsequently analyzed with electron backscattered diffraction (EBSD) and energy-dispersive X-ray spectroscopy (EDS) for phase and crystal orientation mapping. Plan-view EBSD analysis exploited the natural FM surface with no mechanical polishing. A second plan-view aliquot was dissected with a focused ion beam (FIB)–SEM to produce a cross-sectional lamella (Fig. DR2) for scanning/transmission electron microscopy (S/TEM), including high-resolution TEM (HRTEM), single-crystal diffraction, EDS, and integrated EDS–electron energy loss spectroscopy (DualEELS) for geochemical and redox analyses. Sample preparation; SEM, S/TEM, and DualEELS operating conditions; and grain-size quantification methods are detailed in the Data Repository.

TEXTURAL CHARACTERIZATION

The hematite sample comprises two microtextural domains (Fig. 1B). Domain 1 is defined by subparallel to randomly oriented, elongate, intact plates >20–50 µm from the FM surface (Figs. 1A–1C; Fig. DR3). Plate thickness averages 15.1 ± 13.9 µm (2σ), with a 34.1 µm maximum (Fig. DR4A). EBSD phase maps indicate domain 1 is dominantly specular hematite with minor, micrometer-scale, intergranular quartz (Fig. 1C; Fig. DR5).

Domain 2 is the FM volume, with a thickness <20–50 µm, and includes the FM surface (Fig. 1B). Domain 2 comprises polygonal, triple-junction–forming particles lacking defined grain boundaries (Figs. 1D–1E and 2; Fig. DR2). TEM and EBSD data indicate that domain 2 polygonal particles are hematite crystals (Figs. 1F and 2E; Figs. DR6–DR10). A single-crystal diffraction pattern <2 µm from the FM surface yields six-fold coordination and d-spacing consistent with hematite (Fig. 1F). EBSD results indicate some hematite crystals have lamellar twins misoriented at 85°, consistent with rhombohedral twinning (Fig. DR11; Avila et al., 2015). Polygonal grain diameter decreases with increasing distance from the FM surface (Fig. 1E; Fig. DR12). Surface crystals are 0.65 ± 0.75 µm (2σ) in diameter, with a maximum of 2.23 µm (Fig. 2D). At ~10–20 µm from the FM surface, grains are 0.33 ± 0.15 µm (2σ) in diameter, with a 0.54 µm maximum (Fig. DR4C). Polygonal hematite crystals do not exhibit shape preferred orientation (SPO; Fig. 1D; Figs. DR3 and DR13) but are flattened at the FM surface (e.g., Fig. 1D; Fig. DR3F). Grains also lack crystallographic preferred orientation (CPO) and internal subgrains that would be visible in inverse pole figures (Fig. 2F; Figs. DR6–DR10), and they appear relatively dislocation-free in bright-field TEM images (Fig. 3A; grayscale images in Figs. DR14 and DR2G). At the contact between the two domains, some domain 1 specularite plates are mantled by <10-nm-diameter polygonal particles (Fig. DR12).

FAULT MIRROR NANOGEOCHEMISTRY

SEM and S/TEM imaging, EDS, and DualEELS data reveal pervasive, amorphous silica in various textural settings in domain 2. Nanoscale silica occurs at polygonal hematite grain junctions (Figs. 3A, 3B, and 3E), as <5-nm-thick grain-boundary films (Figs. 3D, 3F, and 3G), and as spherical inclusions in hematite (Figs. 3C and 3D). HRTEM images show that the largest interstitial silica zones (~300 nm diameter) are amorphous (Figs. 3B and 3E). A network of semicontinuous, grain-boundary silica nanofilms connects to the larger domains of amorphous silica at the triple junctions. Although EBSD results from the FM surface indicate some interstitial material is quartz (Fig. 2E), comparison of SEM EDS Si maps with the no-solution regions of EBSD phase maps implies some nonindexing silica is amorphous (Figs. DR6, DR9, and DR10).

High-spatial-resolution EBSD phase maps reveal magnetite nanoparticles on the FM surface (Fig. 2E; Figs. DR7 and DR8). They are <50 nm in diameter and occur at the margins and within polygonal hematite crystals. DualEELS suggests the FM surface is also locally coated with reduced Fe (Fe^{2+}) suboxides. Fe L-edge and O K-edge DualEELS spectra acquired at the FM surface are qualitatively more similar, but not identical, to standard magnetite spectra, compared to data acquired away from the FM surface (Fig. DR15). Magnetite is not present in the undeformed domain 1 material (Fig. DR5).

FAULT MIRROR SURFACE TOPOGRAPHY

The FM surface exhibits two networks of polygons (Figs. 2A–2C; Fig. DR13). Polygons

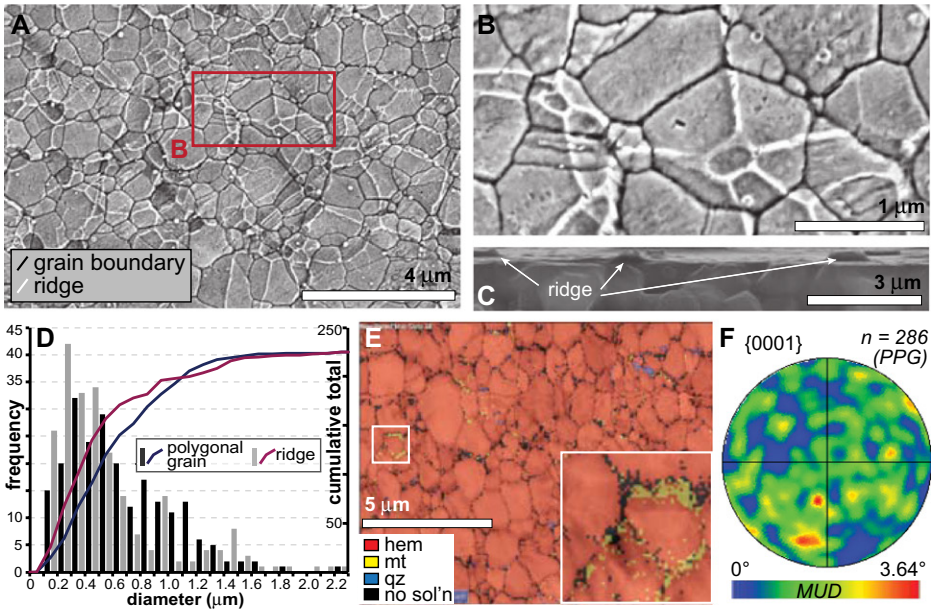

Figure 2. (A,B) Plan-view scanning electron microscope (SEM) secondary election (SE) images of hematite FM surface at two scales showing two polygonal networks. Dark polygons are recessed grain boundaries between adjacent crystals; white polygons are ridge network (visible in C). (C) Cross-sectional SEM image. (D) Distribution of polygonal grain and ridge polygon diameters from SEM-based ImageJ grain-size analysis (n = 225 for each). (E) Electron backscattered diffraction phase map over band contrast image with white box denoting enlarged inset highlighting magnetite nanoparticles; hem—hematite (red), mt—magnetite (yellow), qz—quartz (blue), no soln—no solution (black). (F) Lower-hemisphere, equal-area contoured pole figure indicating no crystallographic preferred orientation to polygonal hematite grains at FM surface. MUD—multiples of uniform density, PPG—point per grain (excluding border grains).

defined by dark-gray lines are recessed regions at grain boundaries between hematite crystals. White lines transecting multiple polygonal crystal faces delineate the second set. Corroborating data sets imply the second is a topographic network of nanometer-high hematite ridges: (1) Both networks yield overlapping mean particle diameters and similar minimum and maximum values (Fig. 2D); (2) rectangular white ridges are consistent with the geometry of rhombohedral twin boundaries observed in some hematite crystals on the preserved FM (Figs. DR11 and DR13); and (3) high-spatial-resolution, long-count SEM EDS point data show no difference in chemical composition between grain faces and the "white" material (Fig. DR16). Although the opposing side of the FM is not preserved, it likely comprises polygonal hematite crystals and interstitial silica observed in domain 2.

EVIDENCE FOR HIGH TEMPERATURES

Multiple lines of micro- to nanotextural and geochemical evidence support high temperatures during FM development. Domain 2 polygonal hematite crystals lack defined grain boundaries, SPO, and CPO; do not exhibit internal subgrains; and appear dislocation free (Figs. 1D, 2F, and 3A). This morphology, suggestive of grain growth and sintering, is similar to textures observed (1) in hematite dry heating experiments to >1000 °C (Vallina et al., 2014); (2) on some Wasatch fault zone (Utah) hematite FMs, where calculated flash temperature rise at 20-µm-diameter asperity contacts is >1200 °C (Ault et al., 2015; McDermott et al., 2017); and (3) on high-gloss experimental faults in carbonate gouge, where coseismic frictional heat is inferred (e.g., Fondriest et al., 2013; Pozzi et al., 2018). In the Wasatch example, polygonal grains are located in clusters reflecting the thermal footprint of localized paleo-asperities (McDermott et al., 2017). In contrast, the textural continuity of polygonal hematite grains from all A16–7 aliquots, covering a total area of ~5 cm^2, implies that temperatures >1000 °C were pervasive in domain 2. Within 15 µm of the FM surface, average and maximum polygonal crystal diameters decrease

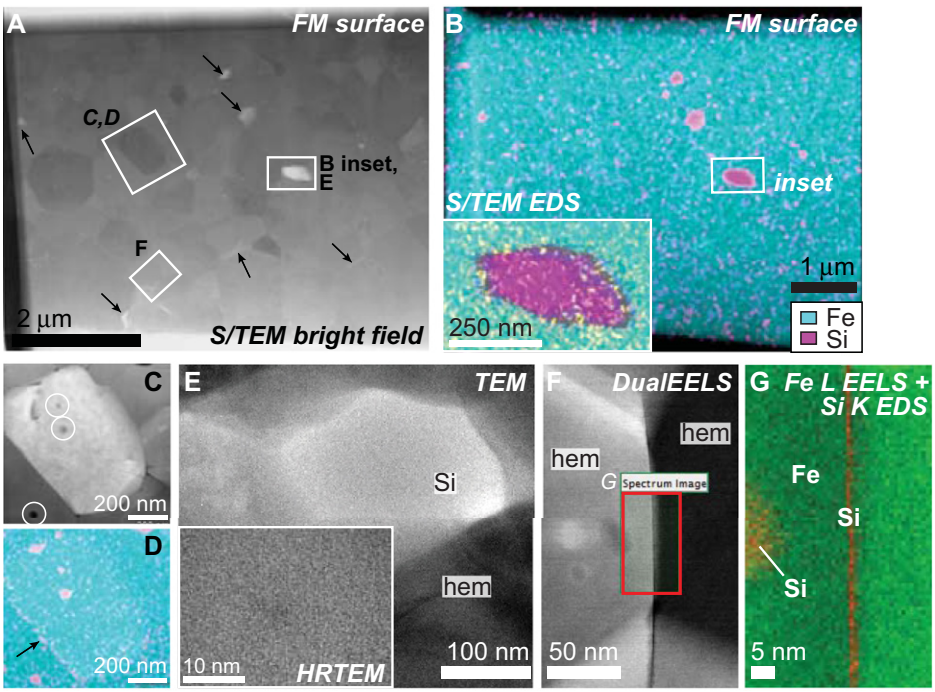

Figure 3. (A) Scanning/transmission electron microscopy (S/TEM) bright-field image showing locations of B inset and C–F. Black arrows denote silica films around polygonal hematite crystals. FM—fault mirror. (B) S/TEM energy dispersive X-ray spectroscopy (EDS) Fe and Si map, where inset shows geochemistry of region in E. (C,D) High-spatial-resolution (HR) S/TEM bright field (C) and complementary EDS (D) images showing spherical silica inclusions (circled in C) and silica along hematite grain boundaries (denoted by black arrow). (E) TEM image of inset in B showing that interstitial silica (Si) within crystalline hematite (hem) is amorphous (inset). (F,G) S/TEM bright-field image of grain boundary between two polygonal hematite crystals (F) and Fe L-edge electron energy loss spectroscopy (DualEELS) and Si K-edge EDS map (G) of zone in F denoted with red box. DualEELS reveals ~5-nm-thick silica film and silica inclusion within hematite.

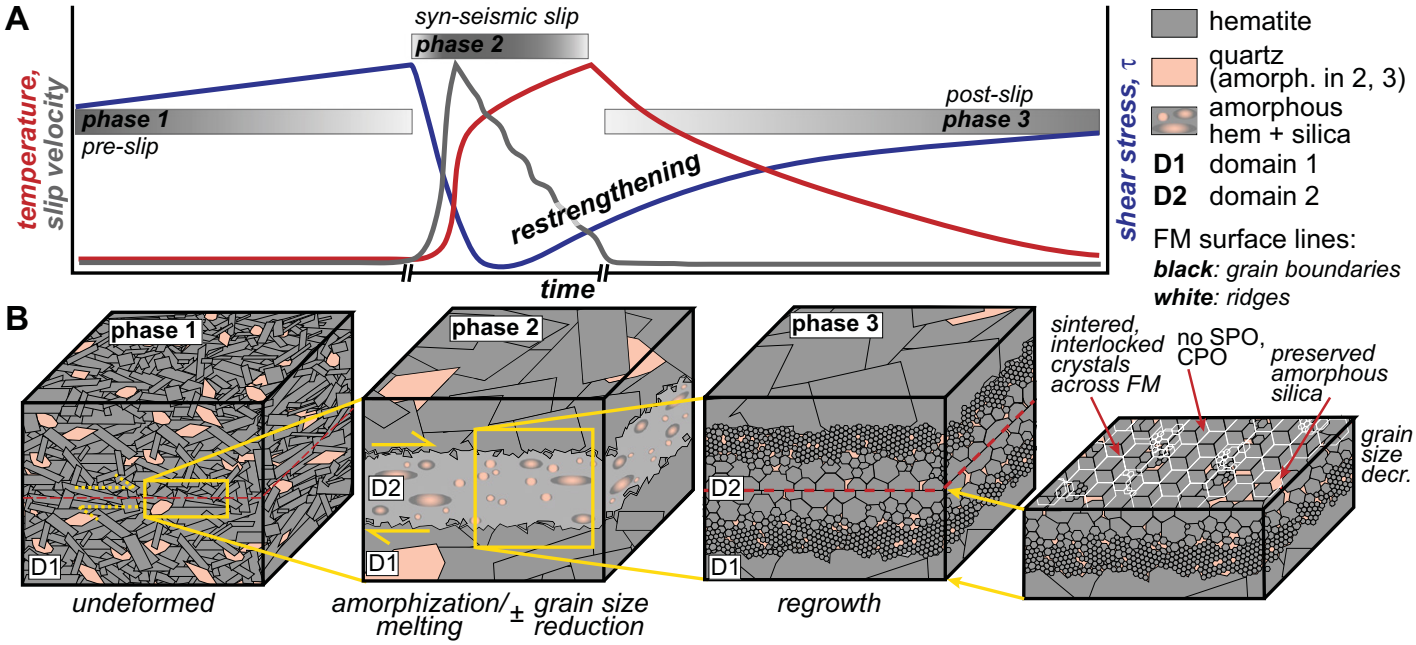

Figure 4. (A) Relative temperature, slip velocity, and shear stress at hematite fault mirror (FM) interface as a function of relative time. (B) Schematic block diagrams illustrating hematite FM textural and inferred rheological evolution associated with conditions in A. Textures and processes are denoted for pre-slip (undeformed; phase 1), syn–seismic slip (phase 2), and post-slip (phase 3). Note diagram scale changes: Phase 2 enlarges a region of phase 1; phase 3 enlarges a region of phase 2. Final diagram is FM surface of phase 3; amorph.—amorphous; decr.—decrease; SPO/CPO—shape/crystallographic preferred orientation.

by a factor of two and four, respectively (Fig. 1E; Figs. DR4 and DR12). This trend reflects a FM-perpendicular thermal gradient in the FM volume. Material at what is now the FM surface experienced the highest temperatures and thus largest crystal growth. In addition, documented magnetite nanoparticles and local Fe^{2+} suboxides on the FM surface support high-temperature Fe reduction during FM development (Fig. 2E; Figs. DR7, DR8, and DR15; Evans et al., 2014).

Amorphous silica implies, but does not require, transient elevated temperatures (e.g., Faber et al., 2014). Although amorphous silica, including interstitial <5-nm-thick grain-boundary films, can form by fluid-mediated and/or dissolution-precipitation processes (Kirkpatrick et al., 2013), which may or may not be coupled with fault slip, the pervasive spherical silica inclusions within neoformed polygonal hematite in domain 2 argue against this interpretation (Figs. 3D, 3F, and 3G). The silica presumably experienced the same high temperatures and thermal gradient documented by hematite nanoparticles in the FM volume.

COUPLED TEMPERATURE-RHEOLOGY EVOLUTION

Evidence for high temperatures implies that this FM developed by seismic slip (Rowe and Griffith, 2015). Figure 4 presents a suite of schematic block diagrams visualizing proposed phases of the FM development (Fig. 4B) with respect to relative slip velocity, shear stress, and temperature (Fig. 4A). Domain 1 preserves undeformed specular hematite and minor intergranular quartz (phase 1).

During seismic slip (phase 2), strain is localized in a <100 µm zone (2× maximum width of domain 2). Temperature rise >1000 °C, perhaps by asperity flash heating during slip initiation (e.g., Rice, 2006), but ultimately by pervasive shear heating (e.g., Ben-Zion and Sammis, 2013) throughout what is now domain 2, results in amorphization or melting of hematite and quartz. Hematite and quartz dry melting temperatures are 1565 °C and 1723 °C, respectively (Spray, 2010). However, increased surface area of domain 2 material via comminution lowers the melting temperature by several hundred degrees Celsius (Lee et al., 2017), thus enhancing frictional weakening mechanisms (Rowe and Griffith, 2015, and references therein). Owing to subsequent transformation of domain 2 material, the role of pre-amorphization grain-size reduction by pulverization or cataclasis, processes commonly invoked during seismic slip (e.g., Reches and Dewers, 2005), is unclear. We note that hematite particles at the margin of domain 2 are >25–75× smaller than the domain 1 plate thickness. Although the hematite is now crystalline, pervasive amorphous silica and silica inclusions imply both phases were transiently amorphous, intermixed but immiscible, and rheologically weak.

Cooling from peak temperatures promotes new mineral growth in a fault-perpendicular thermal gradient (phase 3). In this model, hematite is first to crystallize under low differential stress, supported by the lack of SPO, CPO, and internal strain in polygonal grains, with amorphous silica pinned at grain boundaries. The nanometer-high polygonal ridge network indicates hematite crystals grew into one another and interlocked across the FM surface, which likely formed in the core of the FM volume. Growth of nanoscale crystals, sintering, and twinning are strain hardening (Lu et al., 2005; Luding and Suiker, 2008). These transformations, combined with ubiquitous FM surface topography, contribute to fault healing during slip deceleration and post-slip. Although subsequent deformation can overprint prior textures, we suggest this hematite FM records a single slip event, supported by one set of slickenlines at FM surface margins, the lack of subgrains and CPO, and preserved ridges. The presence of nanotextures that contribute to fault strengthening permit the material to sustain subsequent shear stress but not slip again. Polygonal grains lacking CPO may form by grain boundary sliding and superplastic flow at high temperatures and high strain (De Paola et al., 2015), but the development of the polygonal ridge network supports static grain growth in this example.

Our observations demonstrate the feedback between the FM thermal evolution and rheology during the earthquake cycle. We note that other FMs may form at subseismic slip rates (e.g., Verberne et al., 2013). Differences in observations and interpretations of FM development (cf. Siman-Tov et al., 2013; Pozzi et al., 2018) may depend on preslip material properties (lithology, rock vs. gouge), strain rate, and ambient thermal and pressure conditions during deformation.

IMPLICATIONS FOR THE EARTHQUAKE CYCLE

We suggest that temperature-induced weakening seeds fault restrengthening due to thermal decay and associated rheological changes on some FMs. Processes inferred here complement fault welding and postseismic strength recovery mechanisms documented in experimentally generated pseudotachylytes (Griffith, 2016; Mitchell et al., 2016; Proctor and Lockner, 2016). Our results highlight how thermally induced nanoscale transformations may promote and inhibit earthquake behavior on a broader range of fault surfaces. This has direct implications for strain delocalization, the creation of off-fault damage as a fault system evolves, and the role of nanoscale phenomena during large earthquakes.

ACKNOWLEDGMENTS

This manuscript is dedicated to the late Spencer Titley (University of Arizona, USA, 1928–2019), and we thank him for donating his personal sample for this research. We thank Randy Polson (University of Utah, USA) and Paolo Longo (Gatan Inc, California, USA) for analytical support, Christie Rowe (McGill University, Canada) for feedback on an earlier draft of the manuscript, and helpful comments and edits from three anonymous reviewers that motivated improvements to our contribution. This work was supported by U.S. National Science Foundation (NSF) CAREER grant EAR-1654628 and Southern California Earthquake Center grant 17164 (to Ault). Research made use of University of Utah USTAR shared facilities, supported, in part, by the NSF Materials Research Science and Engineering Centers Program (award no. DMR-1121252).

REFERENCES CITED

Ault, A.K., Reiners, P.W., Evans, J.P., and Thomson, S.N., 2015, Linking hematite (U-Th)/He dating with the microtextural record of seismicity in the Wasatch fault damage zone, Utah, USA: Geology, v. 43, p. 771–774, https://doi.org/10.1130/G36897.1.

Avila, C.F., Lagoerio, L., Barbosa, P.F., and Craca, L., 2015, EBSD analysis of rhombohedral twinning in hematite crystals of naturally deformed iron formations: Journal of Applied Crystallography, v. 48, p. 212–219, https://doi.org/10.1107/S1600576714025928.

Ben-Zion, Y., and Sammis, C.G., 2013, Shear heating during distributed fracturing and pulverization of rocks: Geology, v. 41, p. 139–142, https://doi.org/10.1130/G33665.1.

Blanpied, M.L., Lockner, D.A., and Byerlee, J.D., 1992, An earthquake mechanism based on rapid sealing of faults: Nature, v. 358, p. 574, https://doi.org/10.1038/358574a0.

De Paola, N., Holdsworth, R.E., Viti, C., Collettini, C., and Bullock, R., 2015, Can grain size sensitive flow lubricate faults during the initial stages of earthquake propagation?: Earth and Planetary Science Letters, v. 431, p. 48–58, https://doi.org/10.1016/j.epsl.2015.09.002.

Di Toro, G., Han, R., Hirose, T., De Paola, N., Nielsen, S.B., Mizoguchi, K., Ferri, F., Cocco, M., and Shimamoto, T., 2011, Fault lubrication during earthquakes: Nature, v. 471, p. 494–498, https://doi.org/10.1038/nature09838.

Evans, J.P., Prante, M.R., Janecke, S.U., Ault, A.K., and Newell, D.N., 2014, Hot faults: Iridescent slip surfaces with metallic luster document high-temperature ancient seismicity in the Wasatch fault zone: Geology, v. 42, p. 623–626, https://doi.org/10.1130/G35617.1.

Faber, C., Rowe, C.D., Miller, J.A., Fagereng, A., and Neethling, J.H., 2014, Silica gel in a fault slip surface: Field evidence for palaeo-earthquakes?: Journal of Structural Geology, v. 69, p. 108–121, https://doi.org/10.1016/j.jsg.2014.09.021.

Fondriest, M., Smith, S.A.F., Candela, T., Nielsen, S.B., Mair, K., and Di Toro, G., 2013, Mirror-like faults and power dissipation during earthquakes: Geology, v. 41, p. 1175–1178, https://doi.org/10.1130/G34641.1.

Goldsby, D.L., and Tullis, T.E., 2011, Flash heating leads to low frictional strength of crustal rocks at earthquake slip rates: Science, v. 334, p. 216–218, https://doi.org/10.1126/science.1207902.

Griffith, W.A., 2016, How dynamic weakening makes faults stronger: The role of melting in post-seismic healing: Geology, v. 44, p. 1063–1064, https://doi.org/10.1130/focus122016.1.

Kirkpatrick, J.D., Rowe, C.D., White, J.C., and Brodsky, E.E., 2013, Silica gel formation during fault slip: Evidence from the rock record: Geology, v. 41, p. 1015–1018, https://doi.org/10.1130/G34483.1.

Kuo, L.-W., Song, S.R., Suppe, J., and Yeh, E.-C., 2016, Fault mirrors in seismically active fault zones: A fossil of small earthquakes at shallow depths: Geophysical Research Letters, v. 43, p. 1950–1959, https://doi.org/10.1002/2015GL066882.

Lee, S.K., Han, R., Kim, E.J., Jeong, G.Y., Khim, H., and Hirose, T., 2017, Quasi-equilibrium melting of quartzite upon extreme friction: Nature Geoscience, v. 10, p. 436–441, https://doi.org/10.1038/ngeo2951.

Lu, L., Schwaiger, R., Shan, Z.W., Dao, M., Lu, K., and Suresh, S., 2005, Nano-sized twins induce high rate sensitivity of flow stress in pure copper: Acta Materialia, v. 53, p. 2169–2179, https://doi.org/10.1016/j.actamat.2005.01.031.

Luding, S., and Suiker, A.S.J., 2008, Self-healing of damaged particulate materials through sintering: Philosophical Magazine, v. 88, p. 3445–3457, https://doi.org/10.1080/14786430802438176.

McDermott, R.G., Ault, A.K., Evans, J.P., and Reiners, P.W., 2017, Thermochronometric and textural evidence for seismicity via asperity flash heating on exhumed hematite fault mirrors, Wasatch fault zone, UT, USA: Earth and Planetary Science Letters, v. 471, p. 85–93, https://doi.org/10.1016/j.epsl.2017.04.020.

Mitchell, T.M., Toy, V., Di Toro, G., Renner, J., and Sibson, R.H., 2016, Fault welding by pseudotachylyte formation: Geology, v. 44, p. 1059–1062, https://doi.org/10.1130/G38373.1.

Naranjo, J.A., Henriquez, F., and Nyström, J.O., 2010, Subvolcanic contact metasomatism at El Laco volcanic complex, Central Andes: Andean Geology, v. 37, p. 110–120.

Niemeijer, A.R., Marone, C., and Elsworth, D., 2008, Healing of simulated fault gouges aided by pressure solution: Results from rock analogue experiments: Journal of Geophysical Research–Solid Earth, v. 113, B04204, https://doi.org/10.1029/2007JB005376.

Niemeijer, A.R., Di Toro, G., Griffith, W.A., Bistacchi, A., Smith, S.A.F., and Nielsen, S.B., 2012, Inferring earthquake physics and chemistry using an integrated field and laboratory approach: Journal of Structural Geology, v. 39, p. 2–36, https://doi.org/10.1016/j.jsg.2012.02.018.

Park, C.R., 1961, A magnetite "flow" in northern Chile: Economic Geology and the Bulletin of the Society of Economic Geologists, v. 56, p. 431–436, https://doi.org/10.2113/gsecongeo.56.2.431.

Power, W.L., and Tullis, T.E., 1989, The relationship between slickenside surfaces in fine-grained quartz and the seismic cycle: Journal of Structural Geology, v. 11, p. 879–893, https://doi.org/10.1016/0191-8141(89)90105-3.

Pozzi, G., De Paola, N., Nielsen, S.B., Holdsworth, R.E., and Bowen, L., 2018, A new interpretation for the nature and significance of mirror-like surfaces in experimental carbonate-hosted seismic faults: Geology, v. 46, p. 583–586, https://doi.org/10.1130/G40197.1.

Proctor, B.P., and Lockner, D.A., 2016, Pseudotachylyte increases the post-slip strength of faults: Geology, v. 44, p. 1003–1006, https://doi.org/10.1130/G38349.1.

Reches, Z., and Dewers, T.A., 2005, Gouge formation by dynamic pulverization: Earth and Planetary Science Letters, v. 235, p. 361–374, https://doi.org/10.1016/j.epsl.2005.04.009.

Rice, J.R., 2006, Heating and weakening of faults during earthquake slip: Journal of Geophysical Research, v. 111, B05311, https://doi.org/10.1029/2005JB004006.

Rowe, C.D., and Griffith, W.A., 2015, Do faults preserve a record of seismic slip: A second opinion: Journal of Structural Geology, v. 78, p. 1–26, https://doi.org/10.1016/j.jsg.2015.06.006.

Sibson, R.H., 1992, Implications of fault-valve behaviour for rupture nucleation and recurrence: Tectonophysics, v. 211, p. 283–293, https://doi.org/10.1016/0040-1951(92)90065-E.

Siman-Tov, S., Aharonov, E., Sagy, A., and Emmanuel, S., 2013, Nanograins form carbonate fault mirrors: Geology, v. 41, p. 703–706, https://doi.org/10.1130/G34087.1.

Siman-Tov, S., Aharonov, E., Boneh, Y., and Reches, Z., 2015, Fault mirrors along carbonate faults: Formation and destruction during shear experiments: Earth and Planetary Science Letters, v. 430, p. 367–376, https://doi.org/10.1016/j.epsl.2015.08.031.

Spray, J.G., 2010, Frictional melting processes in planetary materials: From hypervelocity impact to earthquakes: Annual Review of Earth and Planetary Sciences, v. 38, p. 221–254, https://doi.org/10.1146/annurev.earth.031208.100045.

Tornos, F., Velasco, F., and Hanchar, J.M., 2017, The magmatic to magmatic-hydrothermal evolution of the El Laco deposit (Chile) and its implications for the genesis of magnetite-apatite deposits: Economic Geology and the Bulletin of the Society of Economic Geologists, v. 112, p. 1595–1628, https://doi.org/10.5382/econgeo.2017.4523.

Vallina, B., Rodriguez-Blanco, J.D., Brown, A.P., Benning, L.G., and Blanco, J.A., 2014, Enhanced magnetic coercivity of α-Fe_2O_3 obtained from carbonated 2-line ferrihydrite: Journal of Nanoparticle Research, v. 16, p. 2322, https://doi.org/10.1007/s11051-014-2322-5.

Verberne, B.A., Spiers, C.J., Niemeijer, A.R., de Bresser, J.H.P., de Winter, D.A.M., and Plumper, O., 2013, Frictional properties and microstructure of calcite-rich fault gouges sheared at sub-seismic sliding velocities: Pure and Applied Geophysics, v. 171, p. 2617–2640, https://doi.org/10.1007/s00024-013-0760-0.

Yao, L., Ma, S., Platt, J.D., Niemeijer, A.R., and Shimamoto, T., 2016, The crucial role of temperature in high-velocity weakening of faults: Experiments on gouge using host blocks with different thermal conductivities: Geology, v. 44, p. 63–66, https://doi.org/10.1130/G37310.1.

Yasuhara, H., Marone, C., and Elsworth, D., 2005, Fault zone restrengthening and frictional healing: The role of pressure solution: Journal of Geophysical Research–Solid Earth, v. 110, B06310, https://doi.org/10.1029/2004JB003327.

Printed in USA